# *In Silico* Neuro-Oncology: Brownian Motion-Based Mathematical Treatment as a Potential Platform for Modeling the Infiltration of Glioma Cells into Normal Brain Tissue

Markos Antonopoulos and Georgios Stamatakos

*In Silico* Oncology and *In Silico* Medicine Group, Institute of Communication and Computer Systems, National Technical University of Athens, Zografos, Athens, Greece.

**Supplementary Issue: Computer Simulation, Visualization, and Image Processing of Cancer Data and Processes**

**ABSTRACT:** Intensive glioma tumor infiltration into the surrounding normal brain tissues is one of the most critical causes of glioma treatment failure. To quantitatively understand and mathematically simulate this phenomenon, several diffusion-based mathematical models have appeared in the literature. The majority of them ignore the anisotropic character of diffusion of glioma cells since availability of pertinent truly exploitable tomographic imaging data is limited. Aiming at enriching the anisotropy-enhanced glioma model weaponry so as to increase the potential of exploiting available tomographic imaging data, we propose a Brownian motion-based mathematical analysis that could serve as the basis for a simulation model estimating the infiltration of glioblastoma cells into the surrounding brain tissue. The analysis is based on clinical observations and exploits diffusion tensor imaging (DTI) data. Numerical simulations and suggestions for further elaboration are provided.

**KEYWORDS:** *In silico* oncology, computational oncology, tumor growth, glioma invasion, Brownian motion, anisotropic diffusion

**SUPPLEMENT:** Computer Simulation, Visualization, and Image Processing of Cancer Data and Processes

**CITATION:** Antonopoulos and Stamatakos. *In Silico* Neuro-Oncology: Brownian Motion-Based Mathematical Treatment as a Potential Platform for Modeling the Infiltration of Glioma Cells into Normal Brain Tissue. *Cancer Informatics* 2015:14(S4) 33–40 doi: 10.4137/CIN.S19341.

**RECEIVED:** February 05, 2015. **RESUBMITTED:** May 06, 2015. **ACCEPTED FOR PUBLICATION:** May 12, 2015.

**ACADEMIC EDITOR:** J.T. Efird, Editor in Chief

**TYPE:** Review

**FUNDING:** This work has been supported in part by the European Commission under the project Computational Horizons in Cancer (CHIC): Developing Meta- and Hyper-Multiscale Models and Repositories for *In Silico* Oncology (FP7-ICT-2011–9, Grant agreement no: 600841), MyHealthAvatar: A Demonstration of 4D Digital Avatar Infrastructure for Access of Complete Patient Information (FP7-ICT-2011–9–600929), and p-Medicine: Personalized Medicine (FP7-ICT–2009.5.3–270089). The authors confirm that the funder had no influence over the study design, content of the article, or selection of this journal.

**COMPETING INTERESTS:** Authors disclose no potential conflicts of interest.

**CORRESPONDENCE:** gestam@central.ntua.gr



Paper subject to independent expert blind peer review by minimum of two reviewers. All editorial decisions made by independent academic editor. Upon submission manuscript was subject to anti-plagiarism scanning. Prior to publication all authors have given signed confirmation of agreement to article publication and compliance with all applicable ethical and legal requirements, including the accuracy of author and contributor information, disclosure of competing interests and funding sources, compliance with ethical requirements relating to human and animal study participants, and compliance with any copyright requirements of third parties. This journal is a member of the Committee on Publication Ethics (COPE).

Published by Libertas Academica. Learn more about this journal.

## Introduction

Glioblastoma multiforme (GBM) is the most malignant of all brain tumors. Apart from heterogeneity and highly invasive behavior, GBM cells tend to infiltrate the surrounding tissue by solely leaving the main tumor mass and traveling long distances inside the brain.[1] This diffusive behavior of GBM cells is one of the main causes of tumor relapse after resection. Since infiltrating cells are generally not visible by an magnetic resonance imaging (MRI) and an extensive resection may damage surrounding tissue, small populations of such cells are almost always left at the resection margin of GBMs and are widely believed to drive tumor relapse. Therefore, in order to provide quantitative insight into the nonimageable phenomenon of tumor cell invasion, a number of mathematical models have been developed.[2–8] Most of the published mathematical models ignore the anisotropic character of diffusion of glioma cells since truly exploitable tomographic imaging data to this end are rare. In order to enrich the anisotropy-enhanced glioma model weaponry so as to increase the potential of exploiting available tomographic imaging data, we propose a Brownian motion-based mathematical analysis that could serve as the basis for a model estimating the infiltration of glioblastoma cells into the surrounding normal brain tissue. The analysis is based on clinical observations and exploits diffusion tensor imaging (DTI) data. Numerical simulations and suggestions for further elaboration are provided. A realistic model based on the analysis presented could be useful for diagnosis as well as resection and radiotherapy planning.

## Mathematical Modeling of Diffusion

The reaction–diffusion equation has been widely used for modeling the diffusion of tumor cells. In Refs. 2 and 5, the authors assume that tumor cells move from regions of higher to lower densities and exploit the reaction–diffusion equation using an additional term corresponding to the net proliferation of tumor cells:

$$\frac{\partial c}{\partial t} = \nabla \cdot (D \nabla c) + \rho c \quad (1)$$

where $c(x, t)$ is the concentration of glioma cells at time $t$ and location $x$, and $\rho$ reflects the net proliferation of glioma cells. $D$ is the diffusion coefficient, assuming different scalar values on regions of white ($D_w$) and gray ($D_g$) matter, where $D_w > D_g$. In this model, diffusion of tumor cells is mathematically described by the equation

$$\frac{\partial p}{\partial t} = D\left(\frac{\partial^2 p}{\partial x_1^2} + \frac{\partial^2 p}{\partial x_2^2} + \frac{\partial^2 p}{\partial x_3^2}\right) \quad (1a)$$

where $D = D_w$ is the diffusion coefficient in white matter regions, $D = D_g$ is the diffusion coefficient in gray matter regions of the brain, and $x_i$, $i = 1, 2, 3$, denote the three Cartesian coordinates. This model has been widely used throughout the literature. For a review, see Ref. 9. Numerical treatments of Equation (1) can be found in Ref. 7. In Refs. 10 and 11, the authors have expanded this model, introducing in Equation (1) the diffusion coefficient $D$ in the tensorial form, thereby including anisotropy in their models. Measurements of $D$ in the tensorial form were acquired through DTI techniques, which are described in the following section.

The starting point for developing our model is the observation that Equation (1a) is the Fokker–Planck equation corresponding to the stochastic differential equation

$$dx_t = \sqrt{2D} \cdot dB_t \quad (1b)$$

where $B_t$ denotes the standard Brownian motion in $R^3$.[12] Given the initial position $x_o$ of a glioma cell, the distribution of the random variable $x_t$ (ie, the solution of Equation (1b) at time $t$) provides the probability distribution over all possible locations of this cell at time $t$. Given the initial position of a glioma cell in terms of a probability distribution $p(x, 0)$, the probability distribution $p(x, t)$ can be found by the following two equivalent ways: (i) by solving Equation (1a) as a partial differential equation in order to find the evolution of this distribution through time, or equivalently, (ii) by solving the stochastic differential Equation (1b) with initial distribution $p(x, 0)$, in order to find the probability distribution of the random variable $x_t$.

In case we desire to study the movement of many glioma cells constituting a tumor, this notion of distribution is interpreted as follows: integration of $p(x, t)$ over an area $A$ of $R^3$ yields the fraction of the total tumor cell population that is located in $A$.

In the following sections of this article, it will be shown that this point of view provides an intuitive and natural way of modeling anisotropy in the movement of tumor cells.

## Diffusion Tensor Imaging

DTI is an MRI technique measuring the diffusion properties of water molecules along specific directions. This is done by defining an ellipsoid in every voxel of a three-dimensional space which mathematically corresponds to a $3 \times 3$ positive-definite symmetric matrix:

$$D = \begin{bmatrix} D_{xx} & D_{xy} & D_{xz} \\ D_{xy} & D_{yy} & D_{yz} \\ D_{xz} & D_{yz} & D_{zz} \end{bmatrix}$$

This matrix can be decomposed into the following form:

$$D = \begin{bmatrix} u_1 & u_2 & u_3 \end{bmatrix} \begin{bmatrix} \lambda_1 & 0 & 0 \\ 0 & \lambda_2 & 0 \\ 0 & 0 & \lambda_3 \end{bmatrix} \begin{bmatrix} u_1 & u_2 & u_3 \end{bmatrix}^T$$

where $\lambda_1, \lambda_2, \lambda_3$ are the eigenvalues of $D$ (positive, since $D$ is positive definite) and $u_1, u_2, u_3$ are the corresponding orthonormal eigenvectors. The eigenvalues and eigenvectors of $D$ define an ellipsoid with principal axes lying on the directions of $u_1, u_2, u_3$ and having lengths $2\sqrt{\lambda_1}, 2\sqrt{\lambda_2}, 2\sqrt{\lambda_3}$, respectively (Fig. 1).

This ellipsoid, called the diffusion ellipsoid, describes the anisotropic diffusion of dyed water molecules in the specific voxel it refers to. If at the beginning of the observation period, a droplet of water molecules is placed at the center of the ellipsoid, after some time, the front of the diffusing water molecules will form an ellipsoid like the one in Figure 1. This reflects the fact that at a certain location, water molecules do not move toward all directions at equal rates. Diffusion is faster in the larger axis (ie, along the eigenvector corresponding to the larger eigenvalue). For each eigenvector of $D$, the larger the corresponding eigenvalue, the larger the diffusion along its direction. DTI measurements provide this ellipsoid (actually, the principal axes directions and lengths) for each voxel. For a visual representation, see http://commons.wikimedia.org/wiki/File:DTI-axial-ellipsoids.jpg.

Diffusion tensor MRI has been used extensively for tractography *in vivo*. It is widely assumed that water molecules tend to move more easily along white matter tracts; therefore, the fiber bundle of local white matter tracts is assumed to be aligned with the largest axis of the diffusion ellipsoid.[13] Furthermore, measuring the surface of the front of the diffusing water molecules (ie, the surface area of the diffusion ellipsoid) provides a quantity known as apparent diffusion coefficient (ADC), which has been reported to inversely correlate with

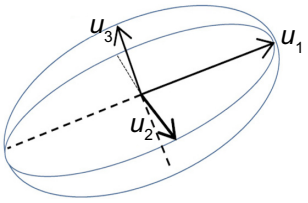


**Figure 1.** The triaxial diffusion ellipsoid. See main text for details.

local cell density.[14,15] Taking into account that brain tumor cells are generally assumed to diffuse toward regions of lower cellular density[2,5] and invade the surrounding tissue by moving along white matter tracts,[1] the diffusion tensor acquired by DTI has been used to describe the diffusion of tumor cells as well.[10,11]

## Derivation of the Model

Our model will use the diffusion tensor measurements provided by DTI to describe the stochastic movement of tumor cells within the brain tissue. Let us assume that we are given a DTI atlas, consisting of the diffusion tensor in each voxel like in Ref. 10. Since the voxel size is of the order 0.5–1 $mm^3$, we will assume that the diffusion tensor is piecewise constant: the diffusion tensor is constant within a voxel and is defined by the measured diffusion ellipsoid of the particular voxel. Thus, supposing that the observation period of the tensor measurement (see before) is $\Delta t$, the movement of a particular water molecule within a voxel can be described by the equation

$$p(x, x_o, \Delta t) = \frac{1}{(2\pi)^{3/2}\det(ULU^T)^{1/2}} \times exp\left(-\frac{1}{2}(x-x_o)^T UL^{-1}U^T(x-x_o)\right) \quad (2)$$

where $p(x, x_o, \Delta t)$ is the probability of a molecule starting at $x_o$ to be at $x$ after time $\Delta t$. $U$ is the matrix whose columns are the orthonormal vectors $u_1, u_2, u_3$ of the diffusion tensor of the voxel, and $L$ is a diagonal matrix with the respective eigenvalues $\lambda_1, \lambda_2, \lambda_3$ as elements of the main diagonal. Thus, given $x_o$, the probability density function of $x$ is a multivariate Gaussian with mean $x_o$ and covariance matrix $ULU^T$. The movement of tumor cells in the same interval $\Delta t$ can be described by the equation

$$p(x, x_o, \Delta t) = \frac{1}{(2\pi)^{3/2}\det(UL_aU^T)^{1/2}} \times exp\left(-\frac{1}{2}(x-x_o)^T UL_a^{-1}U^T(x-x_o)\right) \quad (3)$$

where

$$L_a = \begin{bmatrix} \lambda_1\alpha & 0 & 0 \\ 0 & \lambda_2\alpha & 0 \\ 0 & 0 & \lambda_3\alpha \end{bmatrix} \quad (4)$$

$$L_a^{-1} = \begin{bmatrix} \frac{1}{\lambda_1\alpha} & 0 & 0 \\ 0 & \frac{1}{\lambda_2\alpha} & 0 \\ 0 & 0 & \frac{1}{\lambda_3\alpha} \end{bmatrix} \quad (5)$$

Using Equations (4) and (5), Equation (3) can be written equivalently as

$$p(x, x_o, \Delta t) = \frac{1}{(2\pi)^{3/2}\det(UL_aU^T)^{1/2}} \times \exp\left(-\frac{1}{2}(x-x_o)^T U \begin{bmatrix} \frac{1}{\lambda_1\alpha} & 0 & 0 \\ 0 & \frac{1}{\lambda_2\alpha} & 0 \\ 0 & 0 & \frac{1}{\lambda_3\alpha} \end{bmatrix} U^T(x-x_o)\right) \quad (6)$$

The parameter $\alpha$ is positive and rescales the eigenvalues of the tensor, thereby rescaling conformally the axes of the diffusion ellipsoid. This reflects the fact that tumor cells may tend to move along the axes of the ellipsoid, but do so with a different velocity than water molecules. Since tumor cells move slower than water molecules, we typically expect $\alpha < 1$. Equations (3) and (6) again are Gaussian probability densities for the random variable $x$, ie, the position of a tumor cell after time $\Delta t$ given that the initial position of the cell is $x_o$. Using a standard linear transformation, the random variable $x$ can be equivalently written in the form

$$x = U \begin{bmatrix} \sqrt{\alpha\lambda_1} & 0 & 0 \\ 0 & \sqrt{\alpha\lambda_2} & 0 \\ 0 & 0 & \sqrt{\alpha\lambda_3} \end{bmatrix} Z$$

where $Z$ is a normally distributed random vector with mean $x_o$, and whose covariance matrix is the identity matrix in $R^3$. Equivalently, we can write for the random variable $x - x_o$,

$$x - x_o = U \begin{bmatrix} \sqrt{\alpha\lambda_1} & 0 & 0 \\ 0 & \sqrt{\alpha\lambda_2} & 0 \\ 0 & 0 & \sqrt{\alpha\lambda_3} \end{bmatrix} Z'$$

where $Z'$ is a normally distributed random vector with mean (0, 0, 0) and covariance matrix the identity matrix in $R^3$. This leads us to model the movement in continuous time by the equation

$$x_{t+\Delta\tau} - x_t = U \begin{bmatrix} \sqrt{\alpha\lambda_1} & 0 & 0 \\ 0 & \sqrt{\alpha\lambda_2} & 0 \\ 0 & 0 & \sqrt{\alpha\lambda_3} \end{bmatrix} b$$

where $b$ is a three-dimensional random vector,

$$b \sim \frac{1}{(2\pi)^{3/2}(\Delta\tau)^{3/2}} exp\left(-\frac{b^T b}{2\Delta\tau}\right)$$
$$= \frac{1}{(2\pi)^{3/2}(\Delta\tau)^{3/2}} \exp\left(-\frac{\|b\|^2}{2\Delta\tau}\right)$$

ie, the distribution of $b$ is normal with zero mean and covariance matrix the identity matrix times $\Delta\tau$. This is equivalent to the stochastic differential equation

$$dx_t = \sqrt{a} \cdot U(x) L^{1/2}(x) dB \tag{7}$$

where $B_t$ denotes standard Brownian motion in $R^3$. The matrix $U(x)$ depends on $x$, and its columns are the orthonormal eigenvectors $u_1(x)$, $u_2(x)$, $u_3(x)$ of the diffusion tensor at $x$. The matrix $L^{1/2}(x)$ is diagonal, and its main diagonal entries are the square roots of the eigenvalues $\lambda_1(x)$, $\lambda_2(x)$, $\lambda_3(x)$ of the diffusion tensor at $x$. The parameter $a$ is to be estimated from data. Equation (7) is the model we propose for describing the movement of tumor cells in the brain.

By assuming a twice differentiable diffusion tensor and denoting the probability density function of $x_t$ by $p(x, t)$, the corresponding Fokker–Planck equation describing the evolution of $p(x, t)$ through time is

$$\frac{\partial p(x,t)}{\partial t} = \frac{1}{2}\sum_{i,j=1}^{3}\left[\frac{\partial^2}{\partial x_i \partial x_j}\left(\beta_{i,j}(x)\, p(x,t)\right)\right] \tag{8}$$

where $\beta_{i,j}(x)$ are elements of the matrix

$$\beta(x) = U(x) M^{1/2}(x)\left(U(x) M^{1/2}(x)\right)^T$$

where $M$ is the diagonal matrix with main diagonal entries $\sqrt{a\lambda_1(x)}, \sqrt{a\lambda_2(x)}, \sqrt{a\lambda_3(x)}$.[12] Denoting by $p(x,0)$ the probability distribution of the position of a cell at time 0, we can estimate the probability that the particular cell will lie at a ball of center $x$ at time $t$, by integrating the function $p(x, t)$ on that ball. Sampling from the distribution $p(x, t)$ can give us an estimate on how the cells have spread at the end of the time interval $[0, t]$. Assuming that the diffusion tensor is twice differentiable, solution of Equation (8) could be approximated by numerical methods like finite differences. But DTI provides piecewise constant values for the diffusion tensor, so one should first approximate DTI measurements by a twice differentiable function.

We note that in the case of isotropic diffusion, $U(x)$ is a constant and equals the identity matrix. The eigenvalues $\lambda_1(x)$, $\lambda_2(x)$, $\lambda_3(x)$ are also constants and $\lambda_1(x) = \lambda_2(x) = \lambda_3(x) = \lambda$. In this case, equation reduces to

$$\frac{\partial p(x,t)}{\partial t} = \frac{a\lambda}{2}\left(\frac{\partial^2 p(x,t)}{\partial x_1^2} + \frac{\partial^2 p(x,t)}{\partial x_2^2} + \frac{\partial^2 p(x,t)}{\partial x_3^2}\right)$$

which is the form of the diffusion term in Equation (1a) for isotropic diffusion. A comparison of these equations leads to

$$2D = a\lambda.$$

There are well-known estimates of the diffusion coefficients throughout the literature.[2,5,7] The last equation provides means for estimating the parameter $a$. As seen from this equation, an increased value of the parameter $a$ means a higher diffusion coefficient. Biologically, this corresponds to higher cell motility and a more extended infiltration of glioma cells throughout the brain.

Equation (7) can be written in the form

$$dx_t = \sqrt{a\lambda_1(x)}\, dB_t^1 \cdot u_1(x) + \sqrt{a\lambda_2(x)}\, dB_t^2 \cdot u_2(x) + \sqrt{a\lambda_3(x)}\, dB_t^3 \cdot u_3(x) \tag{7a}$$

where $dB_t^1$, $dB_t^2$, $dB_t^3$ are the one-dimensional components of the three-dimensional vector $dB_t$.

Comparing Equations (1b) and (7a) and taking into account equation $2D = a\lambda$ reveals the connection of our approach with previous ones. Equation (1b) implies that the diffusion ellipsoid is a sphere and that given its initial position, a cell can move along any unit direction with the same probability. By taking into account the axes of the diffusion ellipsoid as provided by DTI and by varying the quantities $\sqrt{a\lambda_1}$, $\sqrt{a\lambda_2}$, $\sqrt{a\lambda_3}$, our model is able to quantify the preferential movement of tumor cells along specific unit directions.

Previous approaches involve numeric integration of Equation (1a). We will not try to solve Equation (8) numerically. Rather, we are going to assume an initial distribution of tumor cells and numerically simulate sample paths from Equation (7) on the interval $[0, t]$. These paths are seen as possible cell trajectories, along which tumor cells infiltrate the surrounding brain tissue. We are going to keep track of the random variable $x_t$, ie, the position of the simulated cell at time $t$ resulting after each simulation. The value of $x_t$ is an approximate sample from the distribution $p(x, t)$.

Through our simulations, we will assume that the matrices $U(x)$ and $L(x)$ are piecewise constants. This assumption is imposed by the minimum voxel size of the DTI technique. Interpolation methods could be used to obtain a smooth version of DTI measurements. Owing to absence of an actual DTI atlas of the human brain, we will not do this in this work.

## Numerical Simulations

To produce sample paths of Equation (7), we will use the Euler–Maruyama[16] numerical scheme:

$$x_{n+1} = x_n + \sqrt{\Delta t}\sqrt{a} U\left(x_n\right) L^{1/2}\left(x_n\right) Z \tag{9}$$

where $Z$ is an $R^3$-valued, normally distributed random variable $Z \sim N(0, I_3)$, and $\Delta t$ is the discretization step. In each iteration,

the matrices $U(x_n)$, $L(x_n)$ are defined by the eigenvalues and eigenvectors of the diffusion tensor of the voxel in which $x_n$ lies.

Scheme (9) has order of strong convergence 1/2. This means that if $\overline{x_T}$ is the solution of Equation (7) at time $T$ as calculated from Equation (9) and $x_T$ is the actual solution of Equation (7) at time $T$, then

$$E \| \overline{x_T} - x_T \| \leq C(\Delta t^{1/2})$$

for some positive constant $C$.[16]

Rewriting Equation (9) in view of Equation (7a) yields

$$x_{n+1} = x_n + \sqrt{\Delta t}\sqrt{a\lambda_1(x_n)}Z_1 \cdot u_1(x_n) + \\ + \sqrt{\Delta t}\sqrt{a\lambda_2(x_n)}Z_2 \cdot u_2(x_n) + \sqrt{\Delta t}\sqrt{a\lambda_3(x_n)}Z_3 \cdot u_3(x_n) \quad (9a)$$

where $Z_1, Z_2, Z_3 \sim N(0,1)$ that is, $Z_1, Z_2, Z_3$ are one-dimensional, independent, and normally distributed random variables and $\Delta t$ is the discretization step.

We will use Equation (9a) for our simulations. It is worth noting that, in view of the previously derived equation, $2D = a\lambda$, since the diffusion coefficient unit is (surface units)/(time units), eg, mm$^2$/h, the quantities $\sqrt{\Delta t}\sqrt{a\lambda_i(x_n)}$, $i = 1, 2, 3$ in Equation (9a) are length units (eg, mm).

Owing to absence of an actual DTI atlas of the brain, simulations were performed using various synthetic diffusion tensors.

Estimates of $D$ were taken from Refs. 2 and 5. A 10-fold variation of $D(D_{max} = 10D_{min})$ was used; we have estimated the quantities $\sqrt{a\lambda_i(x_n)}$, $i = 1, 2, 3$, using the equation $2D = a\lambda$ (Table 1). As for the orthonormal eigenvectors $u_1(x)$, $u_2(x)$, $u_3(x)$ of the local diffusion tensor, we used the following examples:

I. $(1,0,0),(0,1,0),(0,0,1)$,

II. $\left(\frac{\sqrt{2}}{2},0,\frac{\sqrt{2}}{2}\right),(0,1,0),\left(-\frac{\sqrt{2}}{2},0,\frac{\sqrt{2}}{2}\right)$,

III. $\left(\frac{\sqrt{2}}{2},-\frac{\sqrt{2}}{2},0\right),\left(\frac{\sqrt{2}}{2},\frac{\sqrt{2}}{2},0\right),(0,0,1)$, and

IV. $(1,0,0),\left(0,\frac{\sqrt{2}}{2},\frac{\sqrt{2}}{2}\right),\left(0,-\frac{\sqrt{2}}{2},\frac{\sqrt{2}}{2}\right)$.

In each simulation, we have used a population of 40,000 cells, initially distributed according to a standard (non-skewed) Gaussian distribution with small variance (≤1). We have performed simulations for 400, 800, and 1500 hours using a simulation step equal to 1/60 hours. Since each path can be simulated independently, we have parallelized the algorithm on a quad-core computer. The algorithm took about 170 seconds to perform a 1500-hour simulation. Usage of more processors is expected to improve this time.

Simulation results are shown in Figure 2.

Figure 3A and 3B shows isotropic diffusion. The simulation time is 800 hours. For both figures, the diffusion tensor is constant and its eigenvectors consist of triad (I). For Figure 3A, $\sqrt{\Delta t}\sqrt{a\lambda_i(x)} = 0.1\ mm$, $i = 1, 2, 3$. For Figure 3B, $\sqrt{\Delta t}\sqrt{a\lambda_i(x)} = 0.32\ mm$, $i = 1, 2, 3$. As can be seen, diffusion of cancer cells takes place symmetrically along all axes. In Figure 3B, the larger diffusion coefficient results in cells infiltrating a larger area.

Figure 4A and 4B shows anisotropic diffusion. For both simulations, the following synthetic diffusion tensor has been used: For $x_1 \geq 0$, the diffusion tensor is defined by $u_1(x) = \left(\frac{\sqrt{2}}{2},0,\frac{\sqrt{2}}{2}\right), u_2(x) = (0,1,0), u_3(x) = \left(-\frac{\sqrt{2}}{2},0,\frac{\sqrt{2}}{2}\right)$ and $\sqrt{\Delta t}\sqrt{a\lambda_1(x)} = 0.15\ mm, \sqrt{\Delta t}\sqrt{a\lambda_2(x)} = 0.15\ mm, \sqrt{\Delta t}\sqrt{a\lambda_3(x)} = 0.32\ mm$. For $x_1 < 0$, the diffusion tensor is defined by $u_1(x) = (1,0,0)$, $u_2(x) = (0,1,0)$, $u_3(x) = (0,0,1)$ and $\sqrt{\Delta t}\sqrt{a\lambda_1(x)} = 0.25\ mm, \sqrt{\Delta t}\sqrt{a\lambda_2(x)} = 0.1\ mm, \sqrt{\Delta t}\sqrt{a\lambda_3(x)} = 0.1\ mm$. The simulation time is 800 hours and 1500 hours, respectively. Inspection of Figure 4A and 4B reveals the tendency of the cells to move parallel to $\left(-\frac{\sqrt{2}}{2},0,\frac{\sqrt{2}}{2}\right)$ when they lie on the

**Table 1.** Diffusion coefficient and $\sqrt{\Delta t}\sqrt{\alpha\lambda_i(x)}$, $i = 1, 2, 3$, min/max values.

| | MIN | MAX (10×) |
|---|---|---|
| $D\left(\frac{mm^2}{h}\right)$ | 0.0054 | 0.054 |
| $\sqrt{\Delta t}\sqrt{\alpha\lambda_i(x)}$, $i = 1, 2, 3$ $(mm)$ | 0.1 | 0.32 |

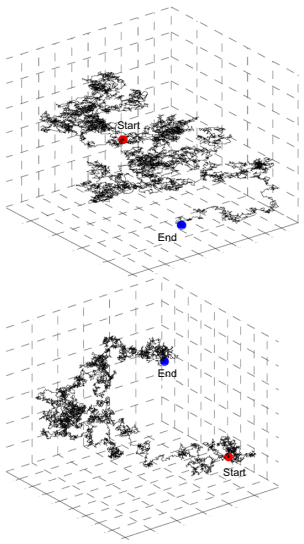


**Figure 2.** Probable (sample) paths of a cell, with starting and ending points. A cell initially located at the start position will perform random, Brownian-like movements described by Equation (7). Sample paths have been obtained by numerical integration of Equation (7). Performing several such simulations and keeping track of the respective end points, one obtains an image of the distribution of cells throughout the brain, as those depicted in Figures 3–5.

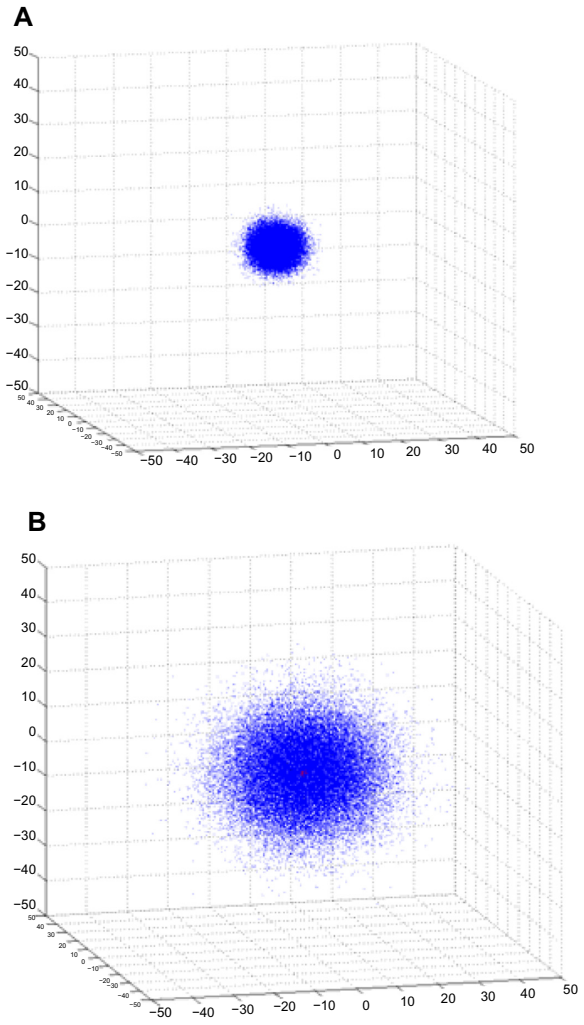


**Figure 3.** Visualization of isotropic diffusion. See text for details.

$x_1 \geq 0$ side and parallel to (1,0,0) when they lie on the $x_1 < 0$ side. Figure 4(C) depicts the projection of Figure 4(B) on the $x_1x_2$ plane. There is a slight wider spread along the $x_2$ axis on the $x_1 \geq 0$ side compared to the one on the $x_1 < 0$ side. This is due to the higher (0.15 to 0.1) value of $\sqrt{\Delta t}\sqrt{a\lambda_2(x)}$ on the $x_1 \geq 0$ side.

Figure 5(A) and (B) also show anisotropic diffusion. The simulation times are 800 hours and 1500 hours, respectively. The following synthetic diffusion tensor has been used: For $x_1 \geq 0$, $x_3 \geq 0$, the diffusion tensor is defined by $u_1(x) = \left(\frac{\sqrt{2}}{2}, 0, \frac{\sqrt{2}}{2}\right)$, $u_2(x) = (0,1,0)$, $u_3(x) = \left(-\frac{\sqrt{2}}{2}, 0, \frac{\sqrt{2}}{2}\right)$ and $\sqrt{\Delta t}\sqrt{a\lambda_1(x)} = 0.32\ mm$, $\sqrt{\Delta t}\sqrt{a\lambda_2(x)} = 0.15\ mm$, $\sqrt{\Delta t}\sqrt{a\lambda_3(x)} = 0.15\ mm$. For $x_1 \geq 0$, $x_3 < 0$, the diffusion tensor is defined by $u_1(x) = \left(\frac{\sqrt{2}}{2}, 0, -\frac{\sqrt{2}}{2}\right)$, $u_2(x) = (0,1,0)$, $u_3(x) = \left(\frac{\sqrt{2}}{2}, 0, \frac{\sqrt{2}}{2}\right)$ and $\sqrt{\Delta t}\sqrt{a\lambda_1(x)} = 0.32\ mm$, $\sqrt{\Delta t}\sqrt{a\lambda_2(x)} = 0.15\ mm$, $\sqrt{\Delta t}\sqrt{a\lambda_3(x)} = 0.15\ mm$. For $x_1 < 0$, the diffusion tensor is defined by $u_1(x) = (1,0,0)$, $u_2(x) = (0,1,0)$, $u_3(x) = (0,0,1)$ and the quantities

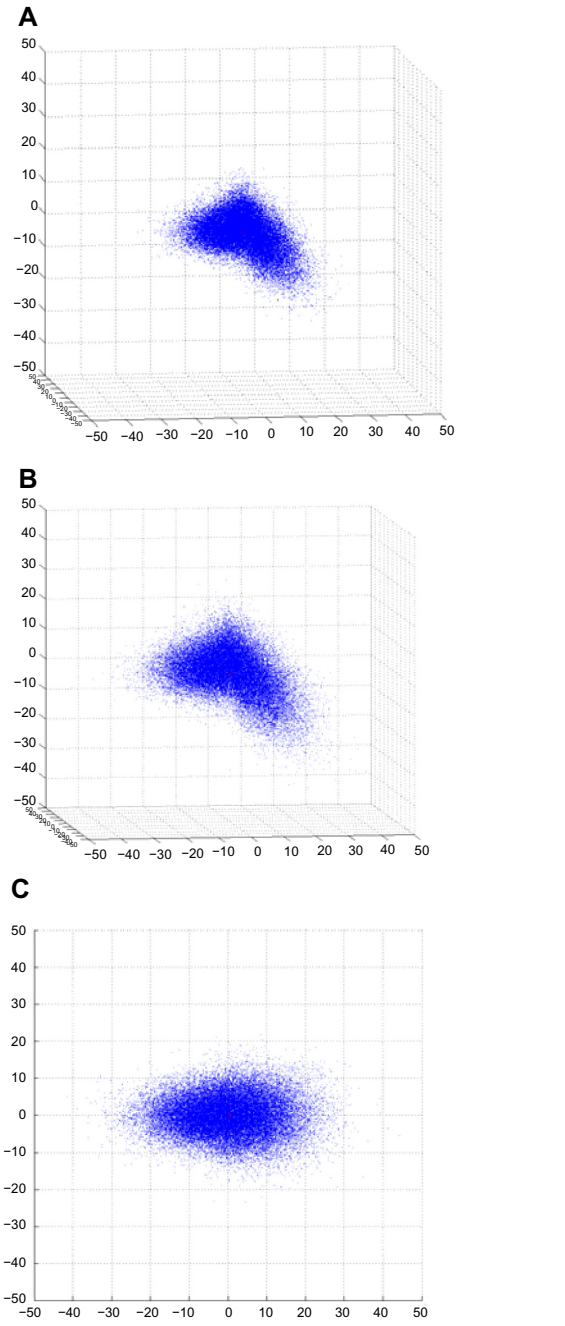


**Figure 4.** Visualization of anisotropic diffusion. See text for details.

$\sqrt{\Delta t}\sqrt{a\lambda_1(x)} = 0.3\ mm$, $\sqrt{\Delta t}\sqrt{a\lambda_2(x)} = 0.2\ mm$, $\sqrt{\Delta t}\sqrt{a\lambda_3(x)} = 0.2\ mm$. In view of Equation (9a), there is a clear tendency of the cells to move parallel to eigenvectors with greater coefficients. In Figure 5(C), we show the projection on the $x_1x_2$ plane. Cells on the $x_1 < 0$ side appear with a smaller density and a wider spread along the $x_1$ axis than those on the $x_1 \geq 0$ side. Again, this is partially explained by the higher value of $\sqrt{\Delta t}\sqrt{a\lambda_2(x)}$ (0.2 to 0.15 mm) on the $x_1 < 0$ side. Cells on the $x_1 < 0$ side tend to move more easily parallel to the $x_2$ axis. Additionally, by comparing the projections on the $x_1$ axis of the vectors $\sqrt{\Delta t}\sqrt{a\lambda_1(x)} \cdot u_1(x)$ of both $x_1 \geq 0$, $x_3 \geq 0$ and

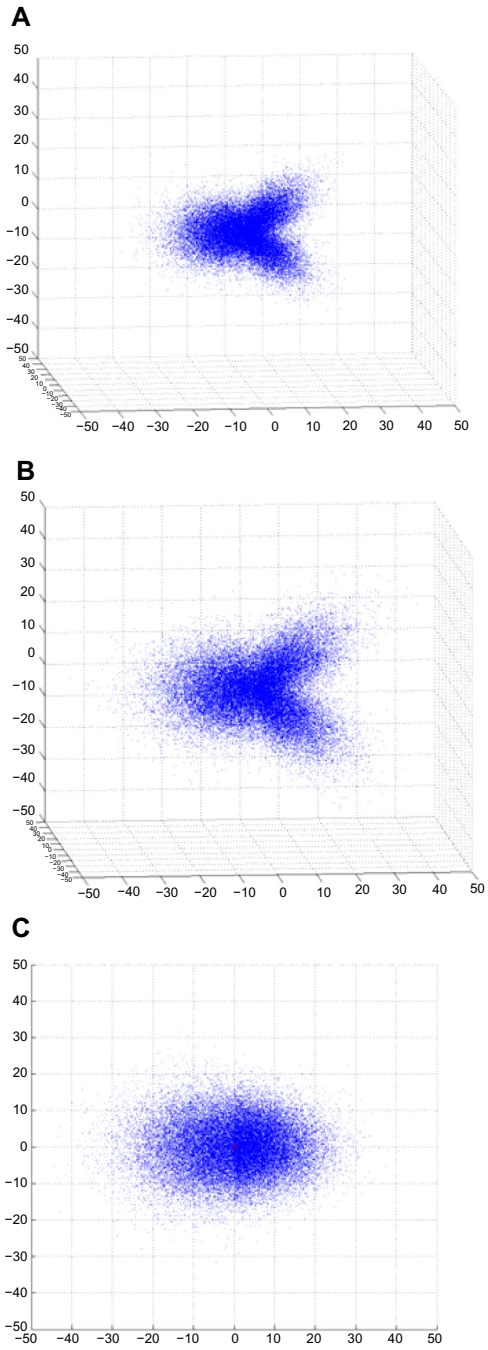


**Figure 5.** Visualization of anisotropic diffusion for a different diffusion tensor. See text for details.

$x_1 \geq 0$, $x_3 < 0$ regions with the value of $\sqrt{\Delta t}\sqrt{a\lambda_1(x)}$ on the $x_1 < 0$ region, we see that in the $x_1 < 0$ region, cells tend to move more easily along the $x_1$ axis as well.

## Discussion

We have modeled the movement of glioma cells in the brain using a stochastic differential equation. Our method relies on the assumption that glioma cells perform a Brownian-like motion while infiltrating the surrounding brain tissue. Our starting observation has been that many popular models describing the same phenomenon do actually imply the same hypothesis; the well known reaction–diffusion Equation (1a) constitutes the Fokker–Planck equation for a simple stochastic differential equation with zero drift and a constant diffusion term. However, it is perceivable that Brownian motion-based models may not be adequate for describing cell movement. Cell movement is affected by several mechanisms, including directed cell motility along gradients of chemoattractant molecules (eg, growth factors, nutrients, cytokines, chemokines) or along gradients of extracellular matrix molecules.[17] These mechanisms are known as chemotaxis and haptotaxis, respectively.[18,19] To the best of the authors' knowledge, *in vivo* measurements concerning such phenomena are not yet feasible. Our approach provides a basis for modeling the random motion of tumor cells, which can be extended and readjusted if such measurements become available. For example, knowledge that tumor cell motility is affected by certain chemotactic or haptotactic gradients can be readily modeled by introducing appropriate nonzero drift terms to Equation (7), each one corresponding to a specific gradient.

We have not included proliferation of cells in the analysis as yet. The latter can be introduced by allowing the sample paths to branch during the time of the simulation in the following way: if a cell located at position $y_o$ divides, sample paths can be produced from Equation (7) with initial position $y_o$, thus producing probable paths for the cells resulting after mitosis. Undoubtedly, this approach implies larger computational burden. However, as previously stated, our model and its simulation algorithm are suitable for parallelization. We leave this for future work.

Since the model is hypothesis oriented, we provide some discussion on how its performance can be assessed, provided that suitable MRI and DTI are available. As described in the previous section, given an initial distribution over possible locations of tumor cells, the model actually produces approximate samples from the distribution $p(x, t)$ of possible locations $x$ of tumor cells at time $t$. We denote these samples by $x_i$, $i = 1, \ldots, N$. The actual distribution of tumor cells $q(x, t)$ can be deduced by a three-dimensional MRI. We let each voxel correspond to a cube and consider the $\sigma$-algebra $\Sigma$ produced by these cubes in $R^3$. Cellular densities of each voxel are normalized to sum to 1.

We use the samples $x_i$, $i = 1, \ldots, N$ to build an approximation of the distribution $p(x, t)$ as follows:

$$\hat{p}(x,t) = \frac{1}{N}\sum_{i=1}^{N} 1_A(x_i) \tag{10}$$

where $1_A$ is the indicator function of the set $A$.

The total variation distance between distributions $\hat{p}(x,t)$ and $q(x, t)$ is

$$\| q(x,t) - \hat{p}(x,t) \|_{TV} = \max_{A\in\Sigma} | q(A,t) - \hat{p}(A,t) | \tag{11}$$

Small variation distance between measured and simulated distributions implies good model performance. Minimization of this distance may also be used for parameter estimation.

## Conclusions – Future Work

We have proposed a novel mathematical treatment for simulating the invasion of glioma tumor cells into the brain. The method consists of simulating probable paths that the tumor cells may follow, using a stochastic differential equation. An inspection of the results obtained so far shows that our approach satisfies basic qualitative characteristics of anisotropic glioma cell diffusion. Therefore, it will be further elaborated – including, ie, the explicit modeling of cell proliferation – in order to finally serve as a tomographic data adaptable diffusion model of glioma invasion and thus eventually improve the simulation of the corresponding biological phenomena.

The proposed model provides a distribution of the glioma cell population throughout the brain. The latter can lead to an estimate of local cell density in any position within the brain. By discretizing the anatomic region of interest through the utilization of a three-dimensional cubic mesh, we can have an estimate of glioma cell density in each cube.

The glioma cells residing within each elementary cube of the mesh can be clustered into subcategories depending on their cell cycle phase status and metabolic activity. At this point, the discrete-entity, discrete-event approach described in Ref. 17 can be recruited in order to simulate the response of glioma to treatment, such as radiotherapy and/or chemotherapy.

## Acknowledgments

Fruitful discussions with Stefaan W. Van Gool, Joost Dejaegher, Lien Solie, and Sofie van Cauter, Medical School, Catholic University of Leuven, Leuven, Belgium as well as Dimitra Dionysiou, ICCS – National Technical University of Athens, Athens, Greece are duly acknowledged. A preliminary version of part of this work has been published as part of the Proceedings of the 2014 6th International Advanced Research Workshop on *In Silico* Oncology and Cancer Investigation – The CHIC Project Workshop (IARWISOCI), Athens, Greece, Nov. 3–4, 2014.

## Author Contributions

Conceived and designed the experiments: MA, GS. Analyzed the data: MA, GS. Wrote the first draft of the manuscript: MA. Contributed to the writing of the manuscript: GS. Agree with manuscript results and conclusions: MA, GS. Jointly developed the structure and arguments for the paper: MA, GS. Made critical revisions and approved final version: MA, GS. Both authors reviewed and approved of the final manuscript.

## REFERENCES

1. Claes A, Idema AJ, Wesseling P. Diffuse glioma growth: a guerilla war. *Acta Neuropathol*. 2007;114(5):443–58.
2. Swanson KR, Alvord EC Jr, Murray JD. A quantitative model for differential motility of gliomas in grey and white matter. *Cell Prolif*. 2000;33(5):317–29.
3. Clatz O, Sermesant M, Bondiau PY, et al. Realistic simulation of the 3-D growth of brain tumors in MR images coupling diffusion with biomechanical deformation. *IEEE Trans Med Imag*. 2000;24(10):1334–46.
4. Clatz O, Bondiau PY, Delingette H, et al. "Brain tumor growth simulation," Institut National de Recherche en Informatique et en Automatique (INRIA), France, Rapport de Recherche, Theme Bio, Systemes Biologiques, Projets Epidaure, No 5187, 2004.
5. Murray JD. *Mathematical Biology II: Spatial Models and Biomedical Applications*. 3rd ed. (Chap. 11). Berlin: Springer; 2011.
6. Konukoglou E, Clatz O, Delingette H, Ayache N. Personalization to brain gliomas characterization and radiotherapy planning. In: Deisboeck T, Stamatakos G, eds. *Multiscale Cancer Modelling*. Boca Raton, FL: Chapman & Hall/CRC Press; 2011:385–406.
7. Giatili SG, Stamatakos GS. A detailed numerical treatment of the boundary conditions imposed by the skull on a diffusion-reaction model of glioma tumor growth. Clinical validation aspects. *Appl Math Comput*. 2012;218(17):8779–99.
8. Roniotis A, Manikis G, Sakkalis V, Zervakis ME, Karatzanis I, Marias K. High grade glioma diffusive modeling using statistical tissue information and diffusion tensors extracted from atlases. *IEEE Trans Inform Tech Biomed*. 2012;16(2):255–63.
9. Harpold HL, Alvord EC Jr, Swanson KR. The evolution of mathematical modeling of glioma proliferation and invasion. *J Neuropathol Exp Neurol*. 2007;66(1):1–9.
10. Jbabdi S, Mandonnet E, Duffau H, et al. Simulation of anisotropic growth of low-grade gliomas using diffusion tensor imaging. *Magn Reson Med*. 2005;54(3):616–24.
11. Stretton E, Geremia E, Menze BH, Delingette H, Ayache N. Importance of patient DTI's to accurately model glioma growth using the reaction diffusion equation. In: Proceedings of ISBI, 2013:1142–5.
12. Grigoriu M. *Stochastic Calculus: Applications in Science and Engineering*. (Chap. 7). Switzerland: Birkhäuser; 2003.
13. Bammer R, Acar B, Moseley ME. In vivo MR tractography using diffusion imaging. *Eur J Radiol*. 2003;45(3):223–34.
14. Chen L, Liu M, Bao J, et al. The correlation between apparent diffusion coefficient and tumor cellularity in patients: a meta-analysis. *PLoS One*. 2013;8(11):e79008.
15. Gauvain KM, McKinstry RC, Mukherjee P, et al. Evaluating pediatric brain tumor cellularity with diffusion-tensor imaging. *AJR Am J Roentgenol*. 2001;177(2):449–54.
16. Kloeden PE, Platen E. *Numerical Solution of Stochastic Differential Equations*. Berlin: Springer; 2013.
17. Stamatakos G. In silico oncology: PART I clinically oriented cancer multilevel modeling based on discrete event simulation. In: Deisboeck TS, Stamatakos GS, eds. *Multiscale Cancer Modeling*. Boca Raton, FL: Chapman & Hall, CRC; 2011. [ISBN 9781439814406].
18. Brockmann MA, Ulbricht U, Grüner K, Fillbrandt R, Westphal M, Lamszus K. Glioblastoma and cerebral microvascular endothelial cell migration in response to tumor-associated growth factors. *Neurosurgery*. 2003;52(6):1391–9.
19. Ziu M, Schmidt NO, Cargioli TG, Aboody KS, Black PM, Carroll RS. Glioma-produced extracellular matrix influences brain tumor tropism of human neural stem cells. *J Neurooncol*. 2006;79(2):125–33.